Hierarchically-Structured and Mechanically-Robust Hydrogel Electrolytes for Flexible Zinc-Iodine Batteries

Yun Tan, Ruixi Liao, Yongbiao Mu, Li Dong, Xingmei Chen, Yu Xue, Ziman Zheng, Fucheng Wang, Zhipeng Ni, Jin Guo, Huicun Gu, Yafei Wang, Zongbao Wang, Lin Zeng,* and Ji Liu*

Hydrogel electrolytes have been widely explored in aqueous zinc-iodine batteries (AZIBs), in light of their intrinsic strong water-retention capability and superior flexibility of hydrogel network. However, hydrogel-based AZIBs are still facing challenges due to the inferior ionic conductivity, dendrite formation, and corresponding fatigue-induced damage. Herein, a hydrogel electrolyte is designed and engineered with preferentially aligned porous structures, where Zn^{2+} can promptly transport along the pores. AZIBs fabricated from the hydrogel electrolyte exhibited distinct cycling stability over 1,000 h (500 cycles) at 0.5 mA cm^{-2}. Moreover, in light of the substantially improved mechanical robustness, the hydrogel electrolyte network remained intact over a 27,000-cycle charging/discharging test at 5 A g^{-1}, with a slight change in capacity, surpassing most previously reported AZIBs. Such kind of hydrogel electrolyte-based AZIBs can be further explored as the flexible power system for wearable devices, enabling significantly accelerated wound healing through electrical stimulation over the epidermal wounds. This work sheds light on hydrogel electrolytes design for long-life aqueous zinc-based batteries, with great potential as power systems for wearable and implantable devices.

Y. Tan, R. Liao, Y. Mu, L. Dong, X. Chen, Y. Xue, Z. Zheng, F. Wang, Z. Ni, H. Gu, Y. Wang, L. Zeng, J. Liu
Department of Mechanical and Energy Engineering
Southern University of Science and Technology
Shenzhen 518055, China
E-mail: zengl3@sustech.edu.cn; liuj9@sustech.edu.cn
J. Guo, Z. Wang
School of Materials Science and Chemical Engineering
Ningbo University
Ningbo 315211, China
L. Zeng
SUSTech Energy Institute for Carbon Neutrality
Southern University of Science and Technology
Shenzhen 518055, China
J. Liu
Shenzhen Key Laboratory of Intelligent Robotics and Flexible
Manufacturing Systems
Southern University of Science and Technology
Shenzhen 518055, China

1. Introduction

Zinc-based rechargeable batteries have received widespread attention for their inherent advantages such as safety, high theoretical capacity, low cost, and environmental friendliness, with great potential in large-scale energy storage devices.[1,2] Among these zinc-based batteries, aqueous zinc-iodine batteries (AZIBs) are promising as one of the next-generation long-lasting power systems, in light of the abundant natural iodine resources ($\approx$55 µg L^{-1} in seawater), large specific capacity (over 200 mA h g^{-1} based on I_2/I^-), and high energy efficiency (>80%).[3–5] However, conventional aqueous electrolytes are consisted of a large amount of water (>95%), which are accompanied with severe zinc electrode corrosion,[6] formation of zinc dendrites,[7,8] and transmembrane contamination of iodine ions, leading to safety risks associated with dramatic capacity deterioration and short circuit.[9–11] As an alternative, hydrogel electrolyte-based AZIBs exhibit excellent mechanical stability and mitigation of iodine ions shuttle, in light of their intrinsic strong water-retention capability and superior flexibility of hydrogel materials, attributing to a highly improved lifespan and reliability.[12,13] Recent progress in hydrogel electrolytes for AZIBs, such as polyacrylic acid (PAA),[14,15] anionic polyacrylamide (PAM),[11,16] and poly(2-acrylamido-2-methyl-1-propanesulfonic acid sodium salt) (PAMPS),[4] can effectively block the active water molecules and coordinate with Zn^{2+}, thereby homogenizing the ion flux and distribution of Zn^{2+}, thus inhibiting the growth of zinc dendrites. However, these hydrogel electrolytes are still facing challenges, such as intrinsic brittleness (i.e., toughness below 0.5 MJ m^{-3}).[11,15]

Most recently, various strategies have been reported to improve the mechanical robustness of hydrogel electrolytes, such as increasing the chemical or dynamic crosslinking density, engineering phase-segregation as the physical crosslinking sites, or formation of the double network.[15,17–19] However, the substantial increase in crosslinking modalities is always accompanied with inhibition of ion conduction, and deterioration in electrochemical performance.[15] Therefore, it remains a grand challenge to

**ADVANCED
SCIENCE NEWS**

www.advancedsciencenews.com

**ADVANCED
FUNCTIONAL
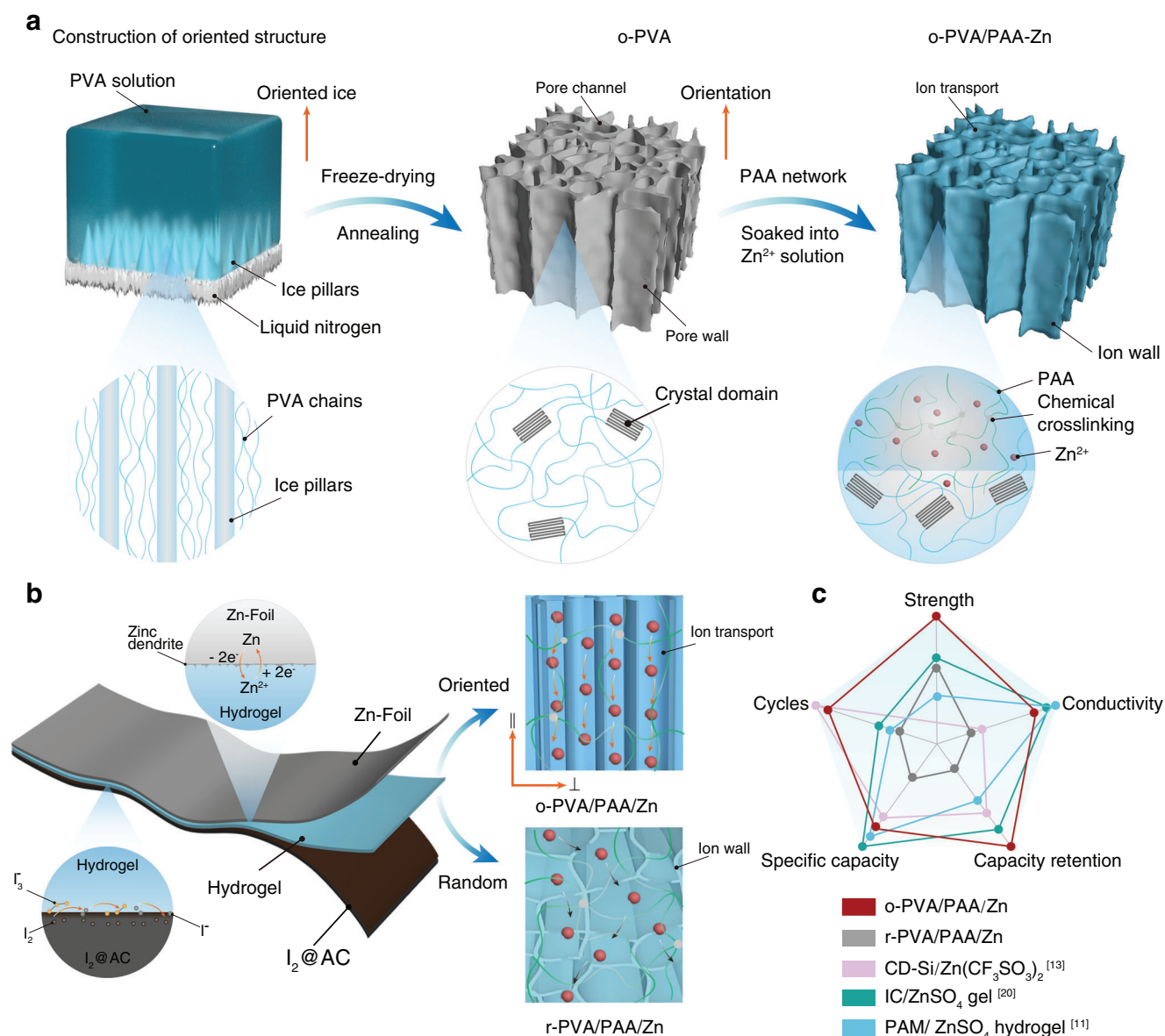MATERIALS**

www.afm-journal.de

Figure 1. Hydrogels with hierarchically-engineered porous structures as electrolytes for AZIBs. a) Schematic illustration of the hydrogel materials engineered with preferentially aligned porous structures from directional freeze casting, thermal annealing, and formation of PAA hydrogel network within the pores. The PVA chains serve as the mechanically robust scaffold with aligned pores, while PAA chains as electrolytes for further complexation with Zn^{2+}. b) Schematic illustration of AZIB assembled with o-PVA/PAA/Zn hydrogel as the electrolyte. The Zn^{2+} transport promptly along the alignment direction with a much higher rate than that within the random pores. Zinc foil and activated carbon loaded with iodine were used as cathode and anode, respectively. c) Radar chart comparing a set of properties, including mechanical strength, ion conductivity, capacity retention, specific capacity, and maximal cycle number of our o-PVA/PAA/Zn hydrogel-based AZIB, together with previously-reported zinc/iodine aqueous state and quasi-solid-state batteries.

engineer hydrogel electrolytes with both excellent mechanical robustness and superior electrochemical properties within one unit through traditional strategies.[12,19] Moreover, during the repetitive charging/discharging cycles (for example, 5000 cycles) of an AZIBs, periodic volumetric expansion/shrinkage, accompanied with the formation of zinc dendrites, could cause fatigue fracture of the hydrogel electrolytes, leading to shuttle effect of iodine ions and potential short-circuit failures.[11,20] Inferior ion transport rate and fatigue-induced damage of hydrogel electrolyte

have been the crucial factors that dominate the lifecycle of these hydrogel-based AZIBs, and hamper their rapid innovations and broad applications.[12,18,19]

Herein, we report a design rationale to fabricate hydrogel electrolytes for AZIBs with preferentially aligned porous structures, enabling the fast and unidirectional transpiration of Zn^{2+} (**Figure 1**). A poly(vinyl alcohol) (PVA) scaffold was fabricated from the freeze-casting technique, followed by functionalizing the pores with a poly(acrylic acid) hydrogel network and then

**ADVANCED
SCIENCE NEWS**

www.advancedsciencenews.com

**ADVANCED
FUNCTIONAL
MATERIALS**

www.afm-journal.de

introducing the Zn^{2+} (o-PVA/PAA/Zn). Inherited from the preferentially aligned porous structures, the Zn^{2+} transportation rate can be increased up to 0.44, while the hydrogel electrolytes exhibited a fatigue threshold up to 1070 J m^{-2}. These unprecedented properties could effectively prevent the formation of dendrites at the zinc anode electrode, but also alleviate the transmembrane contamination of iodine ions, contributing to an unprecedented capacity retention of 95.2%, as well as a high reversible capacity of 110.6 mAh g^{-1} after 27000 cycles at 5 A g^{-1}. Such hydrogel electrolyte-based AZIBs could be further exploited as a flexible power system for the wearable electronics, featuring mechanical compliance, lightweight, low cost, and untethered with cables, and then enable the fast wound healing through electric stimulation.

2. Results and Discussion

To validate our design concept, we used poly(vinyl alcohol) (PVA) as the polymer scaffold in light of its low cost and well-established protocols to engineer its structure and tailor the mechanics,[21–24] while PAA as the electrolyte due to the electrostatic and coordination interactions between PAA and Zn^{2+}.[14,15,25] We first fabricated a PVA hydrogel scaffold through the classical freeze-casting strategy.[21,23,26–29] During the ice-growing process along the vertical direction, PVA chains formed the scaffold with preferentially-aligned porous structures (Figure 1a; Figure S1, Supporting Information). The subsequent thermal annealing treatment significantly increased the crystallinity, leading to the mechanically robust PVA hydrogel scaffolds.[24,26,30,31] Another PAA hydrogel network was introduced into the porous structure (see Experimental part for detailed fabrication process), while interfacial chain entanglement between the PAA and PVA chains imparted the composite structures with robust interface,[32] thus no interfacial failure occurred upon mechanical deformation and/or during the subsequent electrochemical reactions. Finally, the PVA/PAA composite hydrogels were soaked within a $ZnSO_4$ aqueous solution (0.2 mol L^{-1}) until equilibrium, leading to the as-obtained o-PVA/PAA/Zn hydrogel electrolytes. The preferentially-aligned porous structure could significantly facilitate the ion transportation, but also effectively mitigate the side effects, such as homogenizing ion channels and mitigation of zinc dendrite formation at the zinc anodes (Figure 1b), thus improving the reliability of AZIBs. Compared to those previously reported hydrogel electrolytes,[11,13,20] our o-PVA/PAA/Zn hydrogel electrolytes with hierarchically-engineered porous structures possessed highly-improved ion transportation rate, mechanical robustness (i.e., toughness, strength and fatigue resistance), but also superior electrochemical performances (i.e., capacity retention and cycling stability) within the assembled AZIBs (Figure 1c). The combination of these distinct properties within one integrity makes the hydrogel electrolyte a promising candidate as the key component for energy storage devices, striking a balance among ion conductivity, capacity, robustness, efficiency, and durability.

SEM images of the o-PVA/PAA/Zn hydrogel electrolyte evidenced the distinctly aligned structures, with honeycomb-shaped pores size ranging from 1 to 10 μm (**Figure 2a**). The averaged wall thickness increased from ≈400 to 700 nm upon introducing the PAA hydrogel network (Figure 2b; Figure S2, Supporting Information). Quantitative analysis confirmed that water content in-

creased from 66.3 wt% (o-PVA/Zn) to 79.7 wt% (o-PVA/PAA/Zn) hydrogel electrolyte, due to the increased hydrophilicity with the introduction of PAA components (Figure S3, Supporting Information). Upon soaking within the $ZnSO_4$ aqueous solution, Zn^{2+} immediately complexed with the carboxylate groups of PAA chains through electrostatic and coordination interactions (Figures S4–S6, Supporting Information), allowing the Zn^{2+} to gradually diffuse along the aligned porous channels. As a control, hydrogel electrolytes without porous alignment (r-PVA/PAA/Zn) and without PAA component (o-PVA/Zn) were also fabricated for comparison (see Experimental part for detailed fabrication process). Specifically, the concentrations of Zn^{2+} in o-PVA/Zn, o-PVA/PAA-Zn, and r-PVA/PAA/Zn are ≈0.22, 0.21, and 0.15 mol L^{-1}, respectively. Of course, the zinc loading amount could also be rationally tuned by changing the PAA to PVA feeding ratio (Figure S7, Supporting Information).

The microstructures of the PVA/PAA composite hydrogels were further elucidated through small-angle X-ray scattering (SAXS) and wide-angle X-ray scattering (WAXS) analysis (Figure 2c). Preferential alignment of the nanocrystalline domains along the ice-template direction was confirmed with the 2D SAXS and WAXS patterns (Figures S8 and S9, Supporting Information). Notably, the distance between nanocrystalline domains (L) decreased and the size (D) increased upon thermal annealing, similar to our previous finding.[23,26] Mechanical tests confirmed the anisotropic mechanics of the o-PVA/PAA/Zn hydrogel electrolytes, with a fracture strength of 2.42 MPa along the alignment direction (o-PVA/PAA/Zn//), which was 8 times higher than that along the perpendicular direction (o-PVA/PAA/Zn⊥, 0.36 MPa), and three times the random control (r-PVA/PAA/Zn, Figure S10a–c, Supporting Information). Similarly, the toughness reached as high as 7.8 MJ m^{-3}, significantly higher than that along the perpendicular direction (Figure S10d, Supporting Information).

It has been well-established in our previous works that engineered hydrogels with preferential alignment and multi-length scale structural hierarchy could impart them with superior resistance to fatigue crack, thus a prolonged lifetime.[23,24,30,33] Here, we also quantified the fatigue threshold (Γ_0, the minimum fracture energy required for crack extension under cyclic mechanical loadings) of the o-PVA/PAA/Zn hydrogel electrolytes using the single-notch method. Γ_0 along the alignment direction was estimated as high as 1070 J m^{-2}, two orders in magnitude higher than that along the perpendicular direction (30 J m^{-2}) and the random control sample (50 J m^{-2}, Figure 2d–f). Similarly, we have also validated the fatigue threshold by subjecting a notched sample to a 30000-cycle cyclic stretching at an energy release rate (G) of 1070 J m^{-2}, and no crack propagation was detected (Figure 2g; Figure S11, Supporting Information). Such kind of fatigue resistance is highly desirable for the hydrogel electrolytes, which are experiencing periodic yet dramatic volumetric expansion/shrinkage during the cyclic battery charging/discharging process,[18] while fatigue-induced fracture of the hydrogel electrolytes could cause severe outcomes, including electrode corrosion and short-circuit failures.[19]

Ion conductivity and cationic transport rate ($t(Zn^{2+})$) are key parameters dominating the electrochemical performance of the hydrogel-based electrolytes for AZIBs. The Nyquist plots of hydrogel electrolyte in the direction parallel (o-PVA/PAA/Zn//)
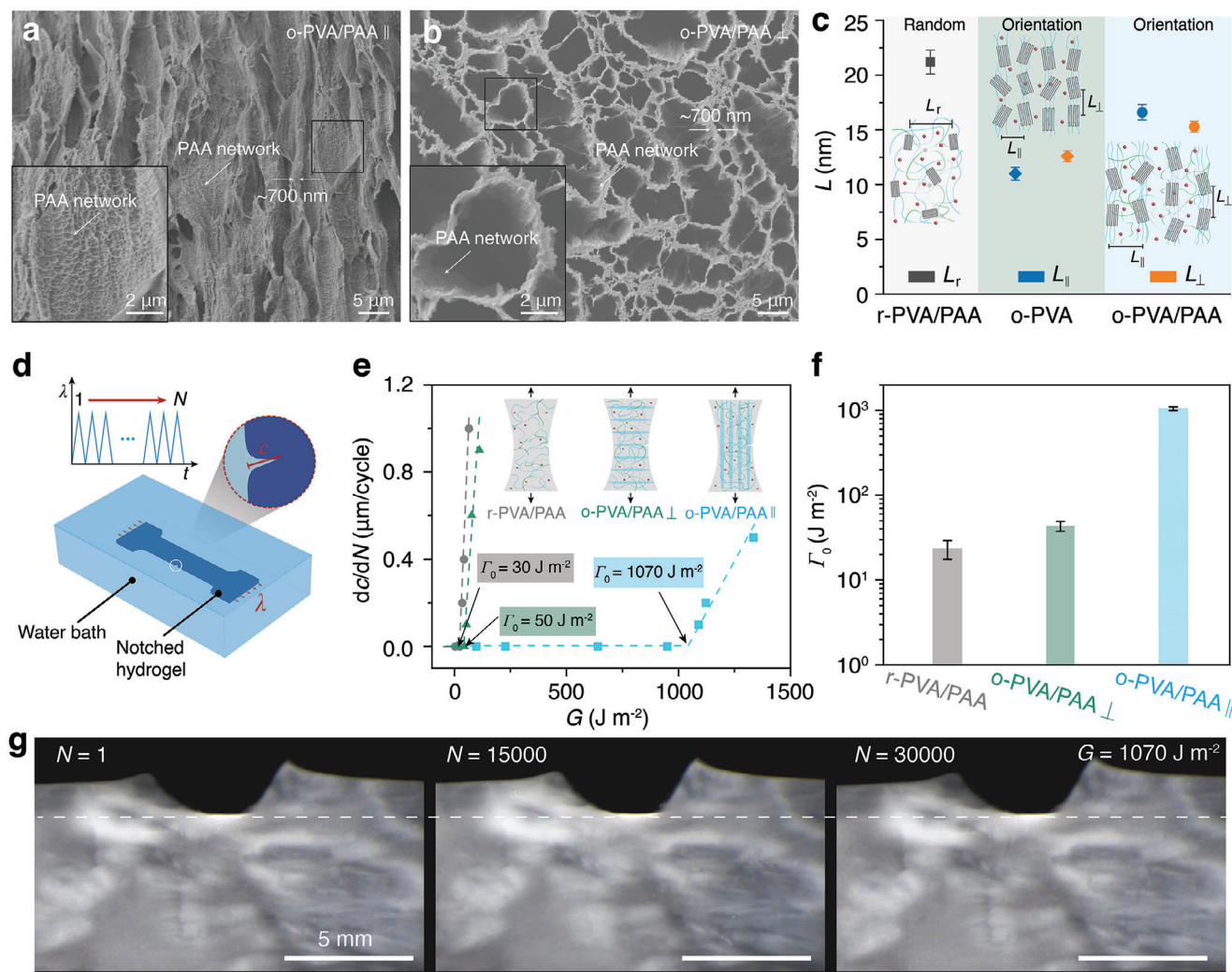
**ADVANCED
SCIENCE NEWS**

www.advancedsciencenews.com

**ADVANCED
FUNCTIONAL
MATERIALS**

www.afm-journal.de

Figure 2. Structural hierarchy and mechanics of the PVA/PAA/Zn hydrogel electrolytes. a,b) Cross-sectional SEM images of the o-PVA/PAA/Zn hydrogel electrolyte at the direction along (//) and perpendicular to (⊥) the alignment direction. Polymer wall thickness of ≈ 700 nm and pore size of 1–10 μm were estimated. c) Summary of distance (L) among the nanocrystalline domains as measured from SAXS analysis for various hydrogel electrolyte samples. d) Schematic illustration of the setup for measuring the fatigue resistance through the classical single-notch method in an aqueous bath. e,f) Plot of crack propagation rate (dc/dN) versus energy release rate (G) for various hydrogel electrolyte samples. g) Validation of the fatigue threshold of 1070 J m^{-2} for the o-PVA/PAA/Zn hydrogel electrolyte sample using a single-notch test at the cycle number of 1, 15000, and 30000. All hydrogel electrolytes were fully swollen in 0.2 M zinc sulfate solution. Data in **c** are presented as means ± standard deviation (S.D.), $n = 3$.

or perpendicular (o-PVA/PAA/Zn⊥) direction were recorded at 25 °C (Figure S12, Supporting Information), while hydrogel electrolytes with random porous structure (r-PVA/PAA/Zn) or without PAA network (o-PVA/Zn) were also tested for comparison. As quantified from the Nyquist plots (**Figure 3a**), a much higher ion conductivity of 2.32 mS cm^{-1} was verified for o-PVA/PAA/Zn//, compared to o-PVA/PAA/Zn⊥ (1.28 mS cm^{-1}) and other two control samples, similar to previously-reported electrolyte systems with preferentially aligned porous structures.[34–36] Zn^{2+} transportation rates of different hydrogel electrolytes, as quantified from the chronoamperometry (CA) test and the Nyquist plots (Figure S13, Supporting Information), were summarized in Figure 3b. A relatively higher Zn^{2+} transport rate (0.44) was detected along the alignment direction, which much higher than the perpendicu-

lar direction (0.21), and also control samples of r-PVA/PAA/Zn (0.28), corroborating the role of aligned pores in modulating the ion transportation of the hydrogel electrolytes.[34,36] In addition, the Zn^{2+} transportation rate of o-PVA/PAA/Zn// was nearly threefolds that of o-PVA/Zn (0.15), which could be attributed to the fact that the PAA chains could tune the ion transportation of Zn^{2+}.[15]

The electrochemical stability window (ESW) is another crucial parameter determining the operation voltage range of a hydrogel electrolyte-based AZIBs, typically tested through the linear sweep voltammetry (Figure 3c). An ESW within the range of 0∼2.50 V versus Zn/Zn^{2+} was confirmed for the hydrogel electrolyte along the alignment direction (o-PVA/PAA/Zn//), slightly wider than that of glass fiber (GF) in zinc sulfate solution (0–2.4 V, 2 M). To further understand the role of aligned porous
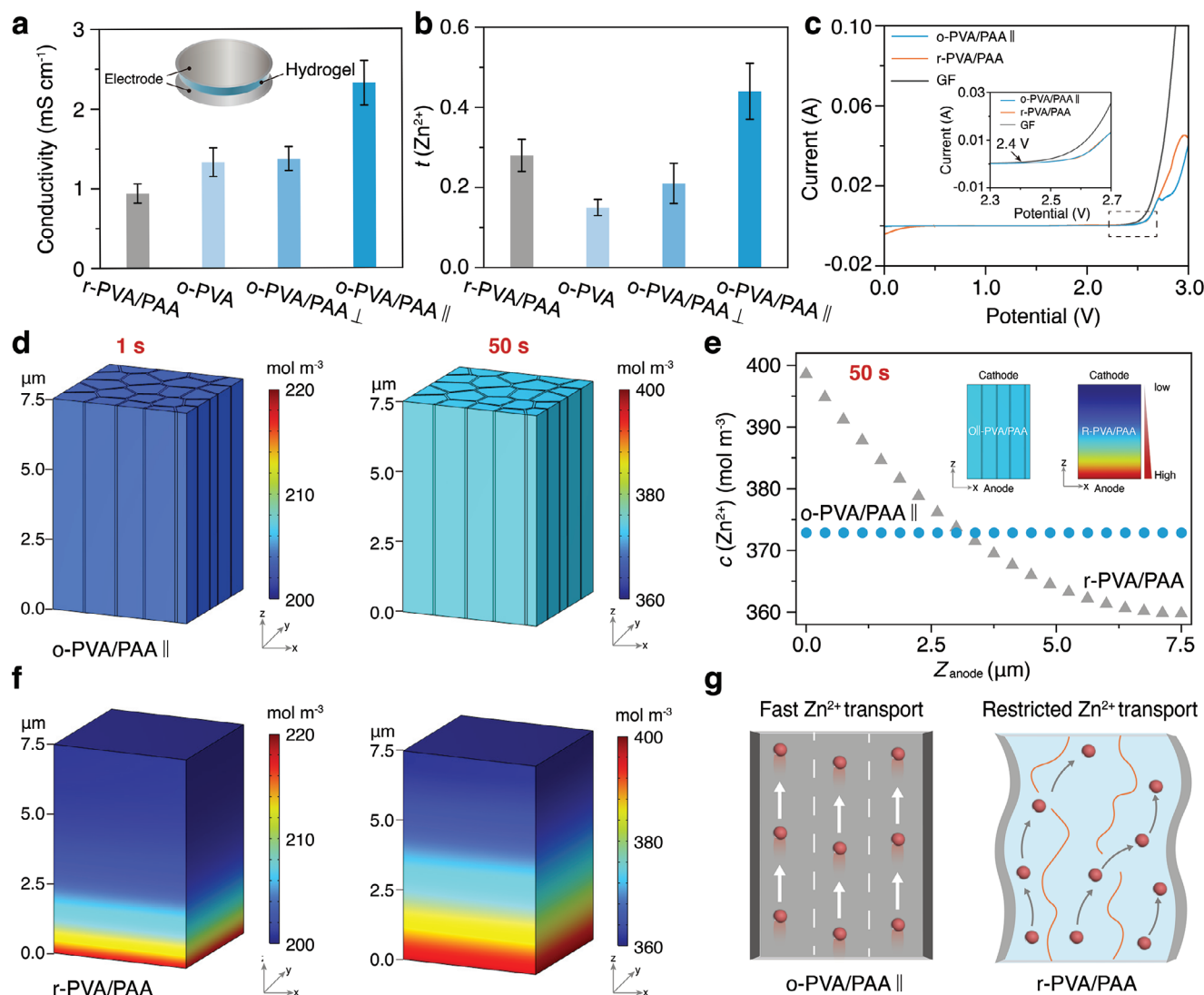
Figure 3. Ion conductivity of the hydrogel electrolytes. a,b) Ion conductivity and Zn^{2+} transport rate in the parallel (o-PVA/PAA/Zn//) or perpendicular (o-PVA/PAA/Zn⊥) direction. Hydrogel electrolytes without random porous structure (r-PVA/PAA/Zn) and without PAA network (o-PVA/Zn) were also tested for comparison. c) The linear sweep voltammetry (LSV) curve of AZIBs assembled with o-PVA/PAA/Zn//, r-PVA/PAA/Zn or glass fiber (GF). d–f) Multi-physics numerical simulation of Zn^{2+} distribution within the o-PVA/PAA/Zn// d) and r-PVA/PAA/Zn f) upon the application of voltage (1.2 V) for 1 and 50 s, respectively; while quantitative Zn^{2+} concentration was plotted for comparison (e). g) Schematic diagram the Zn^{2+} transportation within the o-PVA/PAA/Zn// (left) and r-PVA/PAA/Zn (right). Data in (a) and (b) are presented as means ± standard deviation (S.D.), $n = 3$.

structure in modulating the ion transportation, a multi-physics numerical simulation of the Zn^{2+} distribution in various hydrogel electrolyte samples was conducted to predict the Zn^{2+} diffusion process.[34,35] The anode and cathode were placed at each side of the hydrogel electrolyte, while a voltage of 1.2 V was applied. As shown in Figure 3d,e and Figure S14 (Supporting Information), immediately upon the voltage on within 1 and 50 s, the Zn^{2+} distribution presented obvious homogeneity in the o-PVA/PAA// from the 2D cross-sectional perpendicular patterns. While in sharp contrast, Zn^{2+} preferentially accumulated at the anode of r-PVA/PAA/Zn and o-PVA/PAA/Zn⊥ for both 1 and 50 s voltage on (Figure 3f; Figure S15, Supporting Information), due to the relatively slow ion transportation rate. Moreover, the Zn^{2+} concentration gradient became much

larger across the hydrogel electrolyte after 50 s. The stinking difference in Zn^{2+} concentration at the anode could be interpreted by the difference in ion transportation rate, as determined in Figure 3b,g.

It deserves to be mentioned that preferential accumulation of Zn^{2+} at the anode could lead to the undesired formation of zinc dendrites, a fetal issue associated with the long-term stability of a chargeable battery.[37,38] Previously, most studies exploited the electrolyte engineering strategies, such as electrolyte composition regulation,[8,39] membrane separator,[40,41] and gel electrolytes,[4,15,19] to mitigate the formation of zinc dendrites at the anode, however, the ion transportation and cycling stability of AZIBs are still unsatisfactory.[6,13] In our case, engineering the porous structure to tailor the ion transportation rate could
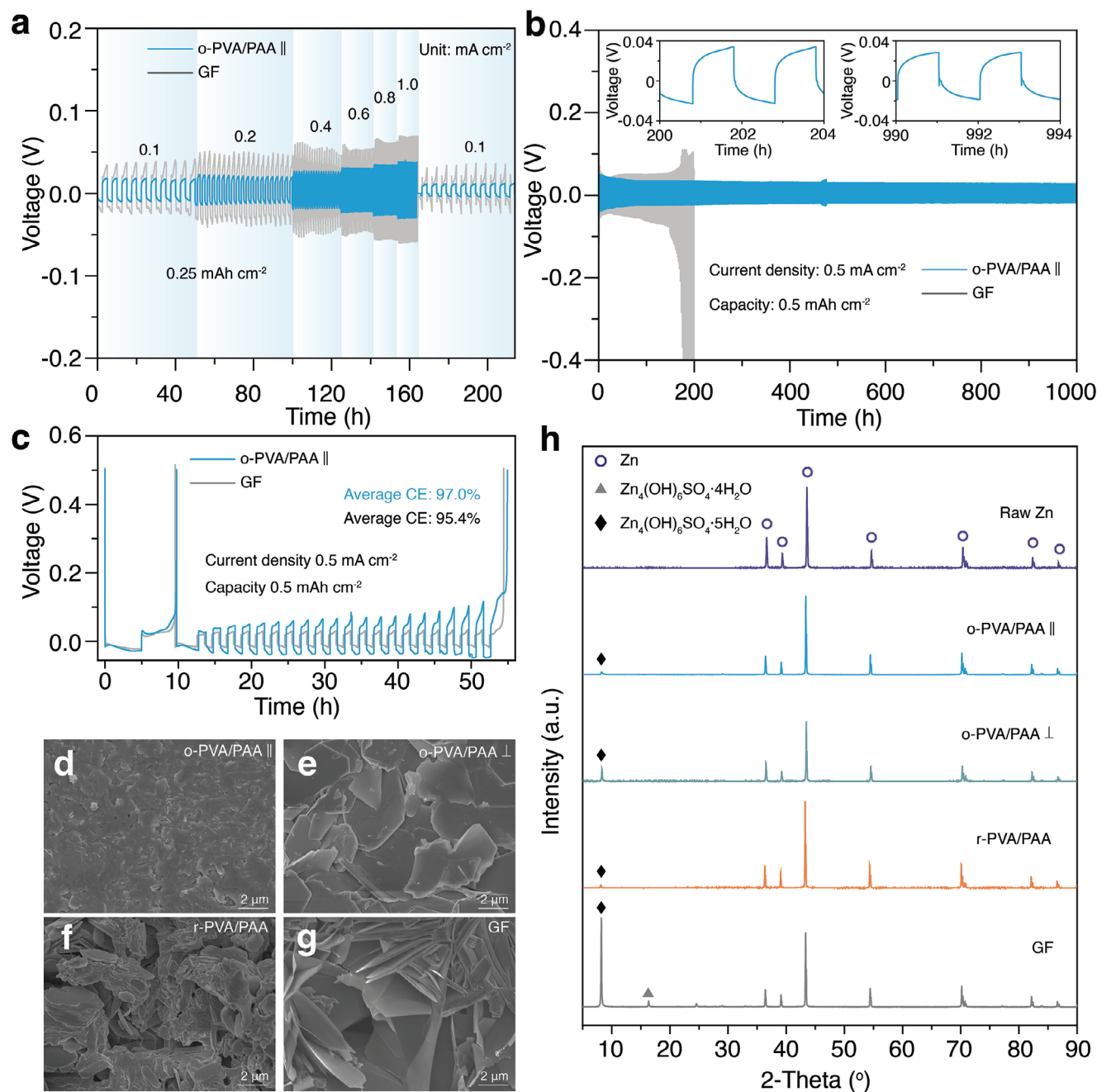
**ADVANCED
SCIENCE NEWS**

www.advancedsciencenews.com

**ADVANCED
FUNCTIONAL
MATERIALS**

www.afm-journal.de

Figure 4. Hydrogel electrolytes within the Zn/Zn symmetric batteries. Rate performance a) and cycling stability b) of the Zn/Zn symmetric batteries using o-PVA/PAA/Zn// as hydrogel electrolyte, while glass fiber was tested as a control. c) Coulombic efficiency of Zn/Cu batteries using o-PVA/PAA/Zn// as hydrogel electrolyte, with glass fiber as a control. d–g) SEM images of zinc anodes after 100-h cycling tests or failure Zn/Zn symmetric batteries as paired with (d) o-PVA/PAA//-100 h, e) o-PVA/PAA/Zn⊥-10 h, f) r-PVA/PAA-80 h, and g) GF-100 h. h) XRD spectra of zinc anodes after 100-h cycling tests or failure Zn/Zn symmetric batteries as paired with different hydrogel electrolytes and GF. Scale bars in (d–g): 2 μm.

effectively accelerate the Zn^{2+} diffusion within the hydrogel electrolyte, electrochemical oxidation, and reduction of Zn/Zn^{2+}, as well as avoidance of Zn^{2+} accumulation at the anode, which could be a promising strategy to prolong the lifespan of chargeable batteries.

To evaluate the stability of hydrogel electrolytes in AZIBs, Zn/Zn symmetric batteries were assembled for rate performance and cycling stability tests. The rate performance result of Zn/Zn symmetric battery based on o-PVA/PAA/Zn// and GF (using 2 M zinc sulfate solution) is displayed in **Figure 4a**. The symmetric battery using o-PVA/PAA/Zn// or GF both exhibited superior cycling stably in the current density range from 0.1 to 1 mA cm^{-2} with a plating/stripping time of 1 h. A significant reduction in overall polarization was observed for the o-PVA/PAA/Zn//,

ADVANCED
SCIENCE NEWS

www.advancedsciencenews.com

ADVANCED
FUNCTIONAL
MATERIALS

www.afm-journal.de

compared to the commonly used GF group, attributing to the superior Zn^{2+} transportation ability. Similarly, symmetric batteries based on r-PVA/PAA/Zn or o-PVA/PAA/Zn⊥ experienced short circuits at a current density of 0.1 mA cm^{-2} (Figure S16, Supporting Information), indicating that inferior Zn^{2+} transportation could significantly deteriorate the long-term cycling stability. We further evaluated the durability of PVA/PAA/Zn// by conducting multiple-cycle charging/discharging on these symmetric AZIBs batteries. Symmetric battery assembled with the o-PVA/PAA/Zn// remained stable for 500 cycles over 1,000 h, at a current density of 0.5 mA cm^{-2} and plating/stripping capacity of 0.5 mAh cm^{-2} (Figure 4b). In sharp contrast, the battery assembled from GF experienced sharply increased polarization after 150 h and suddenly failed at 200 h for 100 cycles. Control samples based on r-PVA/PAA/Zn or o-PVA/PAA/Zn⊥ also failed over 20 cycles in a duration of 40 h at a current density of 0.5 mA cm^{-2} (Figure S17, Supporting Information). It also deserves to be mentioned that the o-PVA/PAA/Zn// group experienced a slight polarization of less than 110 mV over 1000 h (500 cycles), which was substantially smaller than those control groups. Electrochemical reversibility is another indicator for applying in AZIBs. To evaluate the electrochemical reversibility, the Zn/Cu half cells with different hydrogel electrolytes were assembled and examined at 0.5 mA cm^{-2} and 0.5 mAh cm^{-2} for 20 cycles. An average coulomb efficiency of 97.0% was quantified for the o-PVA/PAA/Zn// group, superior than 95.4% of the GF group. All these electrochemical performances corroborated the crucial role of preferentially aligned porous structures in the improved ion conductivity, cycling reversibility, and stability during the zinc deposition/stripping cycles.

We then collected the zinc anode samples for zinc dendrite formation studies, by running a 100-h (50 cycles) cycling on the batteries at a current density of 0.2 mA cm^{-2} and plating/stripping capacity of 0.2 mAh cm^{-2}. The surficial morphologies of the zinc anodes were analyzed with SEM (Figure 4d–g), and a smooth surface was detected for the zinc anode paired with o-PVA/PAA/Zn//. Notably, a significantly rougher surface with the lamellar side products was detected for the GF and r-PVA/PAA groups, indicating the serious corrosion of the zinc anode. To further investigate the formation of side products and the extent of corrosion, ex situ XRD analysis was conducted (Figure 4h). Zinc anode paired with o-PVA/PAA/Zn// displayed the weakest XRD signals regarding the zinc sulfate hydrates, such as $Zn_4(OH)_6SO_4\cdot4H_2O$ and $Zn_4(OH)_6SO_4\cdot5H_2O$, which are the primary corrosion by-products.

The influence of hydrogel electrolytes on the reaction kinetics of the AZIBs was investigated with cyclic voltammetry (CV), at a scan rate of 0.2 mV s^{-1} in the range from 0.6 to 1.6 V (**Figure 5a**; Figures S18 and S19, Supporting Information). Reversible redox peaks at 1.25–1.32 V were recorded in three samples, corresponding to the redox reaction of I^-/I_2. The rate performance was then evaluated by the galvanostatic charge/discharge (GCD) tests (Figure 5b; Figures S20 and S21, Supporting Information). The reversible specific capacities of the o-PVA/PAA/Zn// group were found to be 187.4, 183.1, 180.0, 176.6, 170.2, 166.9, and 164.5 mAh g^{-1} at 1, 2, 4, 10, 15 and 20 C, respectively. Afterward, when the rate was gradually decreased to 1 C, the reversible specific capacity returned to 182.7 mAh g^{-1}. Notably, the reversible specific capacity at a 20 C retained 87.8% of its original value at

a 1 C, marking a significant enhancement in rate capability compared to the o-PVA/PAA/Zn⊥ (0.0%) and the GF group (73.1%). Moreover, AZIBs assembled from o-PVA/PAA/Zn// exhibited the highest specific discharge capacity compared with other samples at 1 C. During the long-term cycling tests, a remarkable capacity retention of 93.2% and reversible capacity of 190 mAh g^{-1} were quantified after 5000 cycles at 0.8 A g^{-1}, superior than the GF with a capacity retention of 56.1%. In sharp contrast, the r-PVA/PAA and o-PVA/PAA/Zn⊥ groups both failed before reaching 1500 cycles (Figure S22, Supporting Information).

The fast ion transportation performance of the batteries was further investigated by long-term GCD at a larger current density of 5 A g^{-1} (Figure 5c,d; Figure S23, Supporting Information). AZIBs made of o-PVA/PAA/Zn// exhibited a distinctly outstanding capacity retention ratio of 95.2% and reversible capacity of 110.6 mAh g^{-1} after 27000 cycles, superior than that of GF (47.6%), o-PVA/PAA/Zn⊥ (53.5%) and r-PVA/PAA/Zn (failed at 5070 cycle). A smooth surface was detected for the zinc anode paired with o-PVA/PAA/Zn//, without the appearance of lamellar zinc dendrites and side products (Figures S24 and S25, Supporting Information). This could be attributed to the fact that o-PVA/PAA/Zn// hydrogel maintained its robust structure and mechanics during the long-cycle charging and discharging process, thus maintaining a superior zinc ion transport rate (Figure S26, Supporting Information). To directly illustrate the superior performance of our hydrogel-based AZIBs, the maximal cycling number and capacity retention ratio were plotting, by comparing our data with several representative works,[6–8,11,13,16,20,37–47] as depicted in Figure 5e. The performance of our o-PVA/PAA/Zn// outperformed most of them, especially in the aspect of capacity retention ratio.

We further evaluated the potential use of our hydrogel electrolyte-based AZIBs as wearable electronics for wound management, as electrical stimulation has been widely established as an effective way to regulate the cellular behaviors, including cell–cell junctions, cell division orientation, and cell migration trajectories, leading to accelerated cell migration and improved wound healing efficacy (**Figure 6a**).[48] A customized circular electrode (i.e., 8 mm in diameter, Figure S27, Supporting Information) was fabricated from 3D-printed silver paste, and then assembled together with the AZIBs (stable output voltage of 1.2 V, Figures S28 and S29, Supporting Information) for the wound repairing in a rat model. The wearable electronics' high flexibility allowed for intact and comfortable contact with the rat's back curvature. A splinted excisional wound model (dimension of 6 mm) was built, and then treated with periodical electrical pulses (duration of 1 h per day, 10 days, Figure 6b), which was termed as the electrical stimulation (ES) group. It is deserved to be mentioned that the rats wearing the AZIBs electronics were able to move freely, similar to the control groups without a device attached but only a gauze bandage (Figure 6c), demonstrating highly desirable electronics for patients' wearable use: mechanical compliance, lightweight, low cost, and untethered with cables. During the 10-day electrical stimulation, a much shorter time of 7 days was needed to reach the complete wound closure than the untreated control group (10 days) (Figure 6d,e). Meanwhile, there was no significant inflammatory response in both the experimental and control groups during electrical stimulation (Figure S30, Supporting Information).
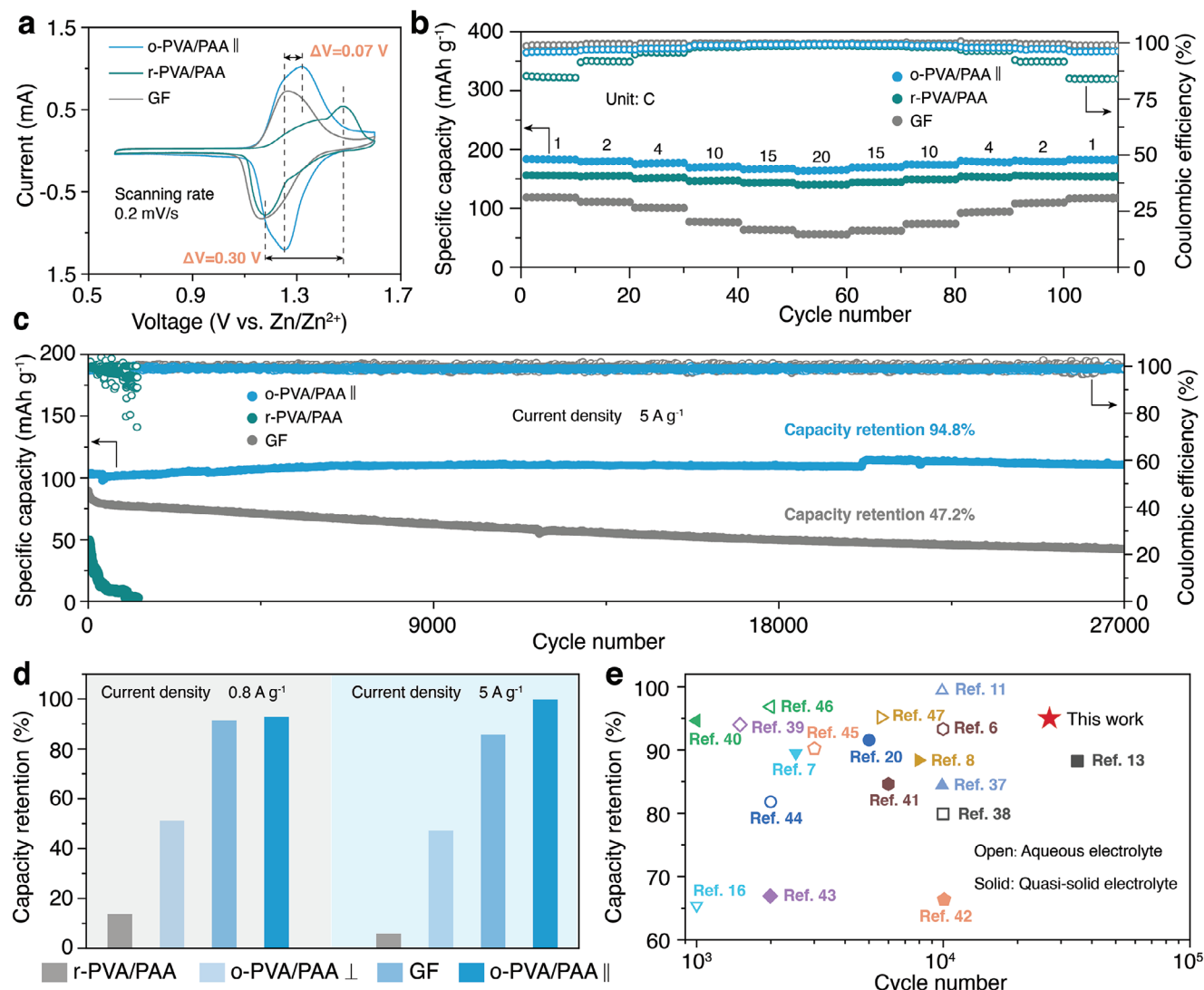
Figure 5. The battery performance of hydrogel electrolyte-based AZIBs. a) Representative CV curves of the AZIBs assembled with o-PVA/PAA/Zn//, r-PVA/PAA or glass fiber at a scanning rate of 0.2 mV s^{-1}. b) Rate performance of the AZIBs. c) Galvanostatic charge-discharge (GCD) profiles of the AZIBs during the long-term cycling tests at a current density of 5 A g^{-1}. d) Summary of capacity retention ratio for AZIBs assembled with o-PVA/PAA/Zn//, o-PVA/PAA⊥, r-PVA/PAA or glass fiber at a current density of 0.8 A g^{-1} or 5 A g^{-1}. e) Comparison chart by plotting the capacity retention ratio against the maximal cycle numbers for our o-PVA/PAA/Zn// hydrogel electrolyte-based AZIBs and previously reported AZIBs.

As shown in Figure 6f, a thicker granulation tissue and narrower wound width were confirmed for the ES group, with abundant collagen bundles deposition in the newly regenerated tissues, resembling structurally to those of the uninjured skin (Figure S31, Supporting Information). For the untreated control group, the thickness of the newly-formed tissue was only 70% of the original size at Day 10, much smaller than the ES group with over 90% (Figure 6g,h). Electrical stimulation has been proven to promote the proliferation and migration of new cells, as well as the formation of neovascularization,[48] here, we have also quantitatively analyzed the density of new-formed blood vessels. As shown in Figure 6i, a significantly higher density of vessels (105 mm^{-1}) was quantified than the untreated control group (50 mm^{-1}). It is also worth to mention that our device did not initiate any irritation during the continuous 10-day wearing with direct contact with the wounds and skins for over 10 days (Figure 6d), as compared with the normal skins, demonstrating a superior biocompatible. Additionally, compared to previously-reported electric stimulation devices relying on coin battery or even tethered power systems,[49,50] our hydrogel-based AIZBs electronics bear the advantages including high capacity, long lifespan, environment friendly, and untethered solution, as well as low cost, making it promising candidate as the versatile power system for various wearable electronics.

3. Conclusion

In summary, we have designed and fabricated a kind of hydrogel electrolytes with hierarchically-engineered porous

ADVANCED
SCIENCE NEWS
www.advancedsciencenews.com

ADVANCED
FUNCTIONAL
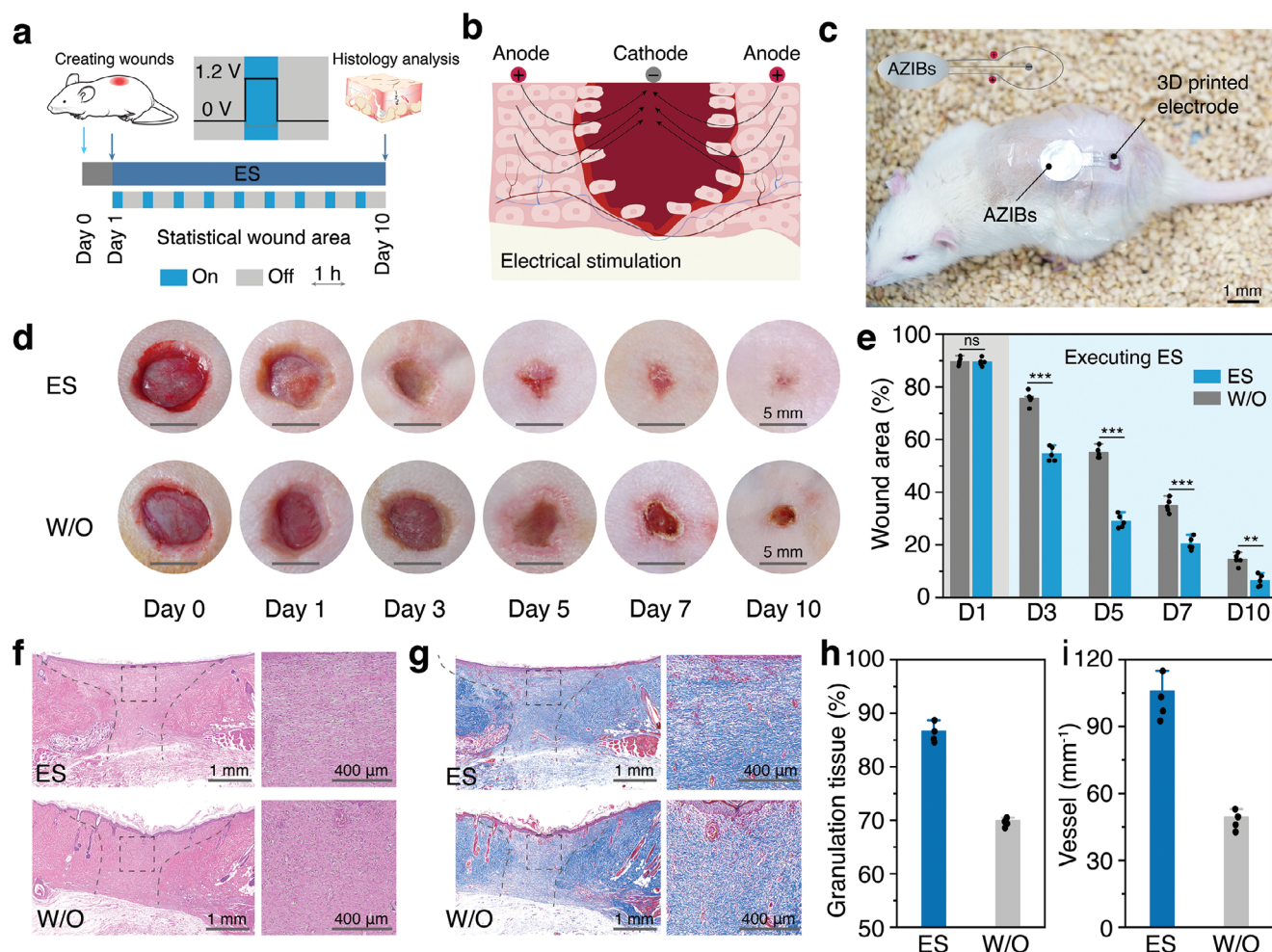**MATERIALS**
www.afm-journal.de

Figure 6. Hydrogel electrolyte-based AZIBs as wearable electronics for wound management. a) Schematic illustration for the working diagram of wound management in a rat model. b) Schematic illustration for electrical stimulation (ES)-accelerated wound healing. c) Photograph of a rat wearing AZIBs wearable electronics for wound management (scale bar: 1 mm). d) Representative images for quantitative analysis of wound closure upon 10-day electrical stimulation. The control group without ES was recorded for comparison. e) Evolution of relative wound area in percentage. f,g) Representative HE and Masson's-stained images for the full-thickness wounds after 10-day treatment. Scale bars: 1 mm and 400 μm. h,i) Summary of granulation tissue thickness and the neovascularization for the ES and control groups. Data in (e,h) and (i) are presented as means ± standard deviation (S.D.), $n = 4$.

structures, while could allow for the highly improved Zn^{2+} transportation rate along the aligned pores. The mechanical strengthening of the polymer scaffold imparted the hydrogel electrolytes with unprecedented fatigue resistance compared to previously reported hydrogel electrolyte systems. Inherited from the superior hierarchical structure and mechanical robustness, the AIZBs based on our hydrogel electrolytes exhibited highly improved electrochemical performances, including cycling stability of zinc symmetric battery over 1, 000 h, capacity retention ratio of full battery with 94.8% (27,000 cycles at 5 A g^{-1}), and mitigated formation of zinc dendrites, surpassing most of previously-reported AIZBs. In light of the mechanical compliance, lightweight, low cost, and high capacity, our hydrogel electrolyte-based AIZBs could be applied as the versatile power systems as wearable electronics, enabling the accelerated wound healing through electric stimulation. It is believed that this work offers a new strategy for fabricating hydrogel electrolyte with the hierarchically-engineered structure, and paves a way for the development of other aqueous batteries with a superior performance.

Supporting Information

Supporting Information is available from the Wiley Online Library or from the author.

Acknowledgements

**ADVANCED
SCIENCE NEWS**

www.advancedsciencenews.com

**ADVANCED
FUNCTIONAL
MATERIALS**

www.afm-journal.de

Conflict of Interest

The authors declare no conflict of interest.

Data Availability Statement

The data that support the findings of this study are available from the corresponding author upon reasonable request.

Keywords

alignment, battery, fatigue resistance, hydrogel electrolytes, porous

[1] X. Jia, C. Liu, Z. G. Neale, J. Yang, G. Cao, *Chem. Rev.* **2020**, *120*, 7795.

[2] W. Sun, F. Wang, B. Zhang, M. Zhang, V. Kuepers, X. Ji, C. Theile, P. Bieker, K. Xu, C. Wang, M. Winter, *Science* **2021**, *371*, 46.

[3] J. Yang, H. Liu, X. Zhao, X. Zhang, K. Zhang, M.-Y. Ma, Z.-Y. Gu, J. Cao, X. Wu, *J. Am. Chem. Soc.* **2024**, *146*, 6628.

[4] J. Yang, Z. Yu, J. Wu, J. Li, L. Chen, T. Xiao, T. Xiao, D. Cai, K. Liu, P. Yang, H. J. Fan, *Adv. Mater.* **2023**, *35*, 2306531.

[5] J. He, Y. Mu, B. Wu, F. Wu, R. Liao, H. Li, T. Zhao, L. Zeng, *Energ. Environ. Sci.* **2024**, *17*, 323.

[6] M. M. Liu, Q. W. Chen, X. Y. Cao, D. X. Tan, J. Z. Ma, J. T. Zhang, *J. Am. Chem. Soc.* **2022**, *144*, 21683.

[7] S. Zhang, J. Hao, H. Li, P. Zhang, Z.-W. Yin, Y. Li, B. Zhang, Z. Lin, S. Qiao, *Adv. Mater.* **2022**, *34*, 2201716.

[8] K. Zhang, Q. Yu, J. Sun, Z. Tie, Z. Jin, *Adv. Mater.* **2024**, *36*, 2309838.

[9] X. Li, N. Li, Z. Huang, Z. Chen, G. Liang, Q. Yang, M. Li, Y. Zhao, L. Ma, B. Dong, Q. Huang, J. Fan, C. Zhi, *Adv. Mater.* **2021**, *33*, 2006897.

[10] Y. Ji, J. Xie, Z. Shen, Y. Liu, Z. Wen, L. Luo, G. Hong, *Adv. Funct. Mater.* **2023**, *33*, 2210043.

[11] X. Jin, L. Song, C. Dai, Y. Xiao, Y. Han, X. Li, Y. Wang, J. Zhang, Y. Zhao, Z. Zhang, N. Chen, L. Jiang, L. Qu, *Adv. Mater.* **2022**, *34*, 2109450.

[12] K. Wu, J. H. Huang, J. Yi, X. Y. Liu, Y. Y. Liu, Y. G. Wang, J. J. Zhang, Y. Y. Xia, *Adv. Energy Mater.* **2020**, *10*, 1903977.

[13] Y. Su, X. Wang, M. Zhang, H. Guo, H. Sun, G. Huang, D. Liu, G. Zhu, *Angew. Chem., Int. Ed.* **2023**, *62*, 2308182.

[14] K. Braam, V. Subramanian, *Adv. Mater.* **2015**, *27*, 689.

[15] Q. Liu, C. Xia, C. He, W. Guo, Z. Wu, Z. Li, Q. Zhao, B. Xia, *Angew. Chem., Int. Ed.* **2022**, *61*, 2210567.

[16] C. Kao, J. Liu, C. Ye, S. Zhang, J. Hao, S. Z. Qiao, *J. Mater. Chem. A* **2023**, *11*, 23881.

[17] Y. Liu, F. Li, J. Hao, H. Li, S. Zhang, J. Mao, T. Zhou, R. Wang, L. Zhang, C. Zhang, *Adv. Funct. Mater.* **2024**, *34*, 2400517.

[18] Z. Chen, T. Shen, M. Zhang, X. Xiao, H. Wang, Q. Lu, Y. Luo, Z. Jin, C. Li, *Adv. Funct. Mater.* **2024**, *34*, 2314864.

[19] Q. Liu, Z. Yu, Q. Zhuang, J. K. Kim, F. Kang, B. Zhang, *Adv. Mater.* **2023**, *35*, 2300498.

[20] Y. Tian, S. Chen, S. Ding, Q. Chen, J. Zhang, *Chem. Sci.* **2023**, *14*, 331.

[21] M. Hua, S. Wu, Y. Ma, Y. Zhao, Z. Chen, I. Frenkel, J. Strzalka, H. Zhou, X. Zhu, X. He, *Nature* **2021**, *590*, 594.

[22] S. Zhu, S. Wang, Y. Huang, Q. Tang, T. Fu, R. Su, C. Fan, S. Xia, P. S. Lee, Y. Lin, *Nat. Commun.* **2024**, *15*, 118.

[23] X. Liang, G. Chen, S. Lin, J. Zhang, L. Wang, P. Zhang, Z. Wang, Z. Wang, Y. Lan, Q. Ge, J. Liu, *Adv. Mater.* **2021**, *33*, 2102011.

[24] S. T. Lin, X. Y. Liu, J. Liu, H. Yuk, H. C. Loh, G. A. Parada, C. Settens, J. Song, A. Masic, G. H. McKinley, X. H. Zhao, *Sci. Adv.* **2019**, *5*, aau8528.

[25] L. Ma, S. Chen, D. Wang, Q. Yang, F. Mo, G. Liang, N. Li, H. Zhang, J. A. Zapien, C. Zhi, *Adv. Energy Mater.* **2019**, *9*, 1803046.

[26] X. Liang, G. Chen, S. Lin, J. Zhang, L. Wang, P. Zhang, Y. Lan, J. Liu, *Adv. Mater.* **2022**, *34*, 2107106.

[27] X. Y. Liang, G. D. Chen, I. M. Lei, P. Zhang, Z. Y. Wang, X. M. Chen, M. Z. Lu, J. J. Zhang, Z. B. Wang, T. L. Sun, Y. Lan, J. Liu, *Adv. Mater.* **2023**, *35*, 2207587.

[28] Z. Zhang, G. Chen, Y. Xue, Q. Duan, X. Liang, T. Lin, Z. Wu, Y. Tan, Q. Zhao, W. Zheng, L. Wang, F. Wang, X. Luo, J. Xu, J. Liu, B. Lu, *Adv. Funct. Mater.* **2023**, *33*, 2305705.

[29] N. F. Zhao, M. Li, H. X. Gong, H. Bai, *Sci. Adv.* **2020**, *6*, eabb4712.

[30] J. Liu, S. Lin, X. Liu, Z. Qin, Y. Yang, J. Zang, X. Zhao, *Nat. Commun.* **2020**, *11*, 1071.

[31] Y. Xue, X. Chen, F. Wang, J. Lin, J. Liu, *Adv. Mater.* **2023**, *35*, 2304095.

[32] J. Kim, G. Zhang, M. X. Shi, Z. G. Suo, *Science* **2021**, *374*, 212.

[33] S. Lin, J. Liu, X. Liu, X. Zhao, *Proc. Natl. Acad. Sci. USA* **2019**, *116*, 10244.

[34] W. Liu, S. W. Lee, D. C. Lin, F. F. Shi, S. Wang, A. D. Sendek, Y. Cui, *Nat. Energy* **2017**, *2*, 17035.

[35] X. Y. Li, Y. Wang, K. Xi, W. Yu, J. Feng, G. X. Gao, H. Wu, Q. Jiang, A. Abdelkader, W. B. Hua, G. M. Zhong, S. J. Ding, *Nano-Micro Lett.* **2022**, *14*, 210.

[36] Z. Y. Ju, T. R. Zheng, J. Calderon, S. Checko, B. W. Zhang, G. H. Yu, *Nano Lett.* **2023**, *23*, 8787.

[37] P. Lin, G. Chen, Y. Kang, M. Zhang, J. Yang, Z. Lv, Y. Yang, J. Zhao, *ACS Nano* **2023**, *17*, 15492.

[38] J. Wu, J. L. Yang, B. Zhang, H. J. Fan, *Adv. Energy Mater.* **2024**, *14*, 2302738.

[39] W. Gao, S. Cheng, Y. Zhang, E. Xie, J. Fu, *Adv. Funct. Mater.* **2023**, *33*, 2211979.

[40] Z. Li, X. Wu, X. Yu, S. Zhou, Y. Qiao, H. Zhou, S. G. Sun, *Nano Lett.* **2022**, *22*, 2538.

[41] H. Yang, Y. Qiao, Z. Chang, H. Deng, P. He, H. Zhou, *Adv. Mater.* **2020**, *32*, 2004240.

[42] W. Li, K. Wang, K. Jiang, *J. Mater. Chem. A* **2020**, *8*, 3785.

[43] W. Shang, J. Zhu, Y. Liu, L. Kang, S. Liu, B. Huang, J. Song, X. Li, F. Jiang, W. Du, Y. Gao, H. Luo, *ACS Appl. Mater. Inter.* **2021**, *13*, 24756.

[44] S. P. Wang, Y. W. Zhao, H. M. Lv, X. H. Hu, J. He, C. Y. Zhi, H. F. Li, *Small* **2023**, *20*, 2207664.

[45] H. L. Pan, B. Li, D. H. Mei, Z. M. Nie, Y. Y. Shao, G. S. Li, X. H. S. Li, K. S. Han, K. T. Mueller, V. Sprenkle, J. Liu, *ACS Energy Lett.* **2017**, *2*, 2674.

[46] L. Q. Zhang, M. J. Zhang, H. L. Guo, Z. H. Tian, L. F. Ge, G. J. He, J. J. Huang, J. T. Wang, T. X. Liu, I. P. Parkin, F. L. Lai, *Adv. Sci.* **2022**, *9*, 2105598.

**ADVANCED
SCIENCE NEWS**

www.advancedsciencenews.com

**ADVANCED
FUNCTIONAL
MATERIALS**

www.afm-journal.de

[47] S. Wang, Z. Huang, B. Tang, X. Li, X. Zhao, Z. Chen, C. Zhi, A. L. L. Rogach, *Adv. Energy Mater.* **2023**, *13*, 2300922.

[48] E. S. Sani, C. H. Xu, C. R. Wang, Y. Song, J. H. Min, J. B. Tu, S. A. Solomon, J. H. Li, J. L. Banks, D. G. Armstrong, W. Gao, *Sci. Adv.* **2023**, *9*, eadf7388.

[49] X. Huang, C. Chen, X. Ma, T. Zhu, W. Ma, Q. Jin, R. Du, Y. Cai, M. Zhang, D. Kong, M. Wang, J. Ren, Q. Zhang, X. Jia, *Adv. Funct. Mater.* **2023**, *33*, 2302846.

[50] H. Ryu, H. M. Park, M. K. Kim, B. Kim, H. S. Myoung, T. Y. Kim, H. J. Yoon, S. S. Kwak, J. Kim, T. H. Hwang, E. K. Choi, S. W. Kim, *Nat. Commun.* **2021**, *12*, 4374.